Investigation of amorphous-SiC thin film deposition by RF magnetron sputtering for optical applications

Didier Chaussende, Vincent Tabouret, Alexandre Crisci, Magali Morais, Stéphane Coindeau, Gregory Berthomé, Manuel Kollmuss, Peter Wellmann, François Jomard, M.A. Pinault-Thaury, et al.

https://doi.org/10.1016/j.mssp.2024.108673

Investigation of amorphous-SiC thin film deposition by RF magnetron sputtering for optical applications

Didier Chaussende [a,*], Vincent Tabouret [a], Alexandre Crisci [a], Magali Morais [a], Stéphane Coindeau [a], Gregory Berthomé [a], Manuel Kollmuss [b], Peter Wellmann [b], François Jomard [c], Marie-Amandine Pinault-Thaury [c], Yaoqin Lu [d], Xiaodong Shi [d], Haiyan Ou [d]

[a] *Univ. Grenoble Alpes, CNRS, Grenoble INP, SIMaP, 38000, Grenoble, France*

[b] *Crystal Growth Lab, Materials Department 6, Univ. of Erlangen-Nürnberg, Germany*

[c] *Groupe d'Etude de la Matière Condensée (GEMaC-UMR8635), CNRS, Université de Versailles St-Quentin-En-Yvelines (UVSQ), Université Paris-Saclay, 45 av des Etats Unis, 78035, Versailles Cedex, France*

[d] *DTU Electro, Technical University of Denmark, DK-2800, KGS, Lyngby, Denmark*

* Corresponding author. SIMaP, 1130 rue de la piscine, BP75, Domaine universitaire, 38402, Saint-Martin d'Hères cedex, France.

E-mail address: didier.chaussende@grenoble-inp.fr (D. Chaussende).

Abstract

Silicon carbide (SiC) is a rapidly emerging material for photonic applications, thanks to its exceptional optical properties. To be used as a waveguide, SiC thin films must be deposited directly on silica at low temperature. Amorphous SiC films were deposited by RF magnetron sputtering using a single source of high-purity poly- crystalline SiC. A systematic study of the chemical, structural and optical properties of the films was carried out, using a combination of XRD, XPS, SIMS, spectroscopic ellipsometry, Raman spectroscopy and UV–Vis absorption spectroscopy. The aim was to link deposition conditions to film properties. By exploring a three-parameter space (RF power, substrate temperature, pressure), we have demonstrated that RF power is the main parameter which controls the entire deposition process and film properties. By simply adjusting the RF plasma power between 150 and 450 W, it is possible to adjust the refractive index at a wavelength of 1.5 μm in the range 2.50–2.75 and vary the bandgap from 2.5 to 1.7 eV. This is attributed to a slight variation in film composition, particularly in terms of Si/C ratio and C–C bond concentration.

Keywords: Silicon carbide Amorphous
Magnetron sputtering Deposition process Optical properties

1. Introduction

Silicon carbide (SiC) is a wide bandgap semiconductor material that is currently entering mass production, associated with the dramatic in- crease in the demand for power electronics, mainly driven by photo- voltaic (PV) conversion and electric vehicles. The entire chain has reached a high technology readiness level, thanks to considerable progress in the size and quality of the 4H–SiC bulk crystals and epitaxial layers [1–3]. It is also rapidly emerging in new photonic applications due to its unique photonic properties, facilitated by advances in micro- and nano-fabrication, achieved in the context of power electronics. Compared to other material platforms, SiC has all the required optical properties: high refractive index, wide bandgap and high second- and third-order nonlinearities, making it ideally suited to photonic inte- grated circuits (PICs) [4]. It also has the unique potential to bridge the gap between classical and quantum photonics, and to technologically advance quantum sensing applications [5]. Many photonic building blocks have already been demonstrated on 4H–SiC material with very good performance, such as highly confined SiC waveguides with excel- lent coupling [6], beam splitters [7], polarization beam splitters [8], optical parametric oscillation [9], optical frequency combs [10] and optical modulators [11].

For integrated optics, amorphous SiC thin films (a-Si_XC_{1-X}) are excellent candidates because they can be deposited at low temperatures, even down to room temperature, and in principle on any substrate. Amorphous SiC films have long been explored, as all their properties - electronic, optical, mechanical, tribological, etc. - can potentially be tuned by adjusting the film composition. In addition, the use of hydrogenated a-SiC:H films opens the way to new properties, as they can be easily doped. Finally, properties can be determined by a combination of deposition strategies, as the properties of a-SiC are strongly linked to the deposition process, and post-processing such as annealing [12–14]. Hydrogenated a-SiC:H films have been extensively explored (see for instance the recent review by Greenhorn et al. [15]) but in its simplest surface contamination or native oXide effect, the measurements were performed after Ar plasma etching of the surface for 60 s, done in situ composition, a-Si_XC_{1-X} alloy has been poorly described, especially just before the measurements. With this procedure, the Si–O, Si–C–O because of intrinsic, weak ordering [16].

Since the first report of a-Si_XC_{1-X} sputtering in 1968 [17], several papers have reported thin film prepared by RF sputtering of SiC targets (see for instance the review by Bullot et al. [14]). As general rules, the deposition rate seems to be mainly governed by RF power, and is only slightly affected by temperature. As expected, the sputtering of poly- crystalline SiC targets in Ar always yields un-hydrogenated material which is nearly stoichiometric. Co-sputtering from silicon and graphite targets allows varying the film's composition, i.e. the silicon/carbon ratio over a wide range. Sputtering in the presence of a reactive gas (H_2, SiH_4, CH_4, etc.) allows effectively controlling the Si/C ratio and incorporating various amounts of hydrogen into the film. Some other papers mentioned highly Si-rich films, with a Si/C ratio decreasing when the applied power to the

target increased and this, even if using a single, stoichiometric SiC target [18].

In this article, we propose to go back to basics, by exploring the relationships between the conditions of the deposition process, here using magnetron sputtering of a single SiC source, and the chemical and optical properties of the film. The aim of this article is to provide a comprehensive picture of these relationships and finally, to give indications for the subsequent optimization of the films according to the application intended.

2. Experimental details

Thin films were deposited by radio-frequency (RF) magnetron sputtering, using an MP500S physical vapor deposition (PVD) system from Plassys. The 3 inches diameter SiC target consisted of a 3 mm thick, high purity polycrystalline SiC plate, prepared by the physical vapor transport (PVT) process. Crystallized from the vapor phase, the plate is mainly composed of large grains of hexagonal polytypes of SiC, with a typical nitrogen residual level in the range of mid 10^{17} cm^{-3} to low 10^{18} cm^{-3}. We can thus consider the target had a stoichiometry of exactly Si/C = 1.00. The plate was then mounted on a copper base. The distance between the target and the substrate was 8.0 cm, kept constant for all the experiments. To improve film homogeneity, a constant rotation of the substrate was used, at a rate of 3 rpm. The substrate holder was of 4 inch in diameter. In this study, three main parameters were considered: the temperature of the substrate (T), which varied from 250 °C to 750 °C, the process pressure (Pr), from 0.1 Pa to 0.9 Pa of argon, and the RF plasma power (Pow) applied to the target, which varied in the 150–450 W range. Depending on the deposition conditions, the thickness of the films could vary between 60 nm and 550 nm. All the other parameters were kept constant.

The following procedure was implemented for all the samples. After loading, the sputtering chamber was first pumped down to a base pressure of 10^{-6} Pa. Then, the substrate surface was exposed to Ar plasma for 10 s for cleaning. 40 sccm of high purity argon (5 N) was used as the ambient atmosphere. Different substrates were used, depending on the characterization requirements. (001) Si wafers, 2 μm thick SiO_2 on Si wafers, (0001) oriented sapphire and glass were used. A systematic investigation of the chemical, structural and optical properties of the films was carried out, using a combination of X-ray diffraction (XRD), X- ray photoelectron spectroscopy (XPS), secondary ion mass spectroscopy (SIMS), spectroscopic ellipsometry, Raman spectroscopy and UV–Vis absorption spectroscopy.

XPS analyses were carried out in a K-Alpha apparatus from Thermo Fisher Scientific. Sample surfaces were irradiated with Al K_α radiation (1486.6 eV) in a UHV chamber (10^{-9} mbar). The ejected electrons were collected by a hemispherical analyzer at 30 eV constant pass energy. The energy scale was calibrated with the C 1s line from the carbon contamination at 285.0 eV. Analyses were carried out at a constant angle (90°) between the sample surface and the analyzer. In order to avoid any components in the Si 2p peak and the C–O component

in the C 1s peak were minimized and sometimes almost negligible, although always considered in the fitting process. The C 1s and Si 2p peaks were fitted using multiple Gaussian functions; the background was removed by the Shirley subtraction method. The different components were fitted using the kinetic energies gathered in Table 1. An example of peak deconvolution is given in Appendix 1. Note that we did not decompose the C–C contribution into two components, sp^3 and sp^2, as was done for instance in Ref. [19]. Here the total C–C bonds are accounted for, without considering the exact nature of the bonds [20].

Table 1. Values of binding energies used for fitting the XPS spectra.

Nature of the components	Binding Energy (eV)
C–Si (C 1s peak)	283.3
C–C (C 1s peak)	284.4
C–O (C 1s peak)	286.3
Si–C (Si 2p peak)	100.8
Si–C–O (Si 2p peak)	102.6
Si–O (Si 2p peak)	103.7

Secondary ion mass spectrometry (SIMS) was used to measure the Si^-/C^- ratio, with the aim of evaluating the Si/C ratio of the film. The SIMS analysis was performed in dynamic mode with a magnetic sector mass spectrometer (IMS7f-CAMECA, Gennevilliers - France). For SiC homoepitaxy, SIMS is usually performed in order to measure the depth distribution of dopants (as nitrogen) and contaminants (like hydrogen) in the films. In routine analysis, the raster size is 150x150 μm^2, meaning that the primary beam (~few µm of diameter) sweeps across the sample surface over a 150x150 μm^2 area. The zone analyzed is restricted to a diameter of 33 µm to avoid crater edge effects. An electronic gate is set to 70 % to reinforce the rejection of edge effects. The analysis chamber is kept under high vacuum (~$5x10^{-10}$ mbar). As the SIMS technique is mostly used in SiC to detect electro-negative impurities, measurements are performed with parameters allowing high sensitivities. Namely, the Cs^+/M^- configuration is classically employed: positive primary ions with a Cs^+ source and detection of negative secondary ions of mass M [21]. The energy of the Cs^+ primary beam is set to 10 keV. Secondary ions are detected in the negative mode by biasing the sample to -5kV, leading to an impact energy of the primary ions of 15 keV and an incidence angle of ~23° with respect to the normal of the sample. We used a primary intensity of 20 nA that leads to a sputtering rate of around 0.26 nm/s in SiC matrix.

We applied this standard SIMS conditions for SiC analysis onto ~40 samples, with low mass resolution settings (usually used to ensure a high level of transmission). $^{12}C^-$ and $^{28}Si^-$ were the only elements

detected. We used multi-hole sample holders to measure 4 samples in the same run. Only one sample holder at a time could be introduced in the anal- ysis chamber. For each introduction of the sample holder, the deflectors from the secondary stage were first initialized, then optimized on the center of each sample before performing the mass calibration of the elements analyzed, followed by the analysis. Each sample was analyzed 2 or 3 times, close to the adjustment crater, to check reproducibility of the measurement in the same area (~1100 μm^2). The goal was to measure the Si^-/C^- ratio (meaning the major elements), while the detection was performed with the Faraday cup which has the advantage of not having dead time. The counting time was 1 s per point. The analysis was stopped at the interface between the SiC layer and the substrate, leading to a total analysis time between 200 and 1800 s, depending on the SiC layer thickness. An example of the SIMS measurement is given in Appendix 2. With such a procedure, SIMS measurements are far more precise than XPS measurements on the Si/C determination, typically more than one order of magnitude (see section 3). Consequently, all the Si/C ratios discussed in the paper have been measured by SIMS.

The amorphous nature of the samples was characterized by X-ray diffraction. Two different set-ups were used to measure the samples: the first one was a PANalytical X'Pert Pro MPD diffractometer, equipped with a 1.8 kW Cu source, with automatic slits providing a 12 x 8 mm^2 illuminated area, and a 1D PiXel detector; the second set-up consisted of a Rigaku Smartlab diffractometer equipped with a 9 kW copper rotating anode source and a HypiX 3000 2D detector for some of the samples. The major advantage of the 2D detector is that it captures a larger area of reciprocal space, enabling the capture of the signal diffracted by crystal planes inclined 15° along the Chi axis with respect to the surface. This made it possible to detect the presence of any crystallites with an orientation which could not be detected by an X-ray diffraction measurement in conventional geometry. Thus, a range of 16°–125° along 2Theta and 30° wide along the Chi axis was collected for several samples.

The thickness and refractive index (RI) of a-SiC layers were estimated by spectroscopic ellipsometry (SE). Measurements were performed on a Semilab SE-2000 tool over a 190–1650 nm range. The optical model used for a-SiC layers formed on both sapphire a-Al_2O_3 and 2.0 μm SiO_2/ c-Si substrates was a stack composed of an effective medium approximation (EMA) layer (roughness) and a bulk a-SiC layer. The dielectric function of a-SiC was modeled using a Tauc-Lorentz law. Absorption spectra were collected in the UV–visible (190–900 nm) range using a Shimadzu - 2501pc double beam spectrophotometer. a-SiC thin films deposited on glass were used for these transmission measurements. Raman analyses were performed on a Renishaw RM1000 spectrometer at 514 nm with a x50 objective. Laser power was adjusted to avoid any heating or modification of the sample. The Raman shifts were systematically calibrated using a Si wafer.

3. Results and discussion

The deposition rate (R_d) was plotted on a 2D map as a function of substrate temperature (T) and plasma power

(P_{ow}) (Fig. 1). Rd increased sharply with the RF power applied to the target, with an almost linear relationship (Fig. 2). For instance, $R_d = 0.8P_{ow}$ at a pressure of 0.9 Pa. When the pressure was lower, for example 0.1 Pa, the deposition rate was much higher and depended even more on RF power. Again, assuming a linear dependence, $R_d = 1.4P_{ow}$ at 0.1 Pa. To achieve a measurable deposition rate, the minimum RF power required (X-axis intercept) was around 100 W and 45 W at pressures of 0.9 Pa and 0.1 Pa, respectively. Although the absolute values depended on the sputtering machine, the trends had already been reported in the literature [22–28]. They were attributed to a higher species ejection rate when the RF power applied to the target increased. By lowering the pressure, the ejection rate was enhanced and the collision frequency between the target and the substrate considerably reduced, which contributed to increasing deposition efficiency. Indeed, the mean free path should be around 1 cm at 0.9 Pa and 250 °C, and 25–30 cm at 0.1 Pa and 750 °C. The first set of conditions (higher pressure) imposed a mean free path which was much shorter than the target to substrate distance (8 cm in our case), whereas the second set of conditions corresponded to a much larger mean free path. The effect of temperature was much weaker and requires a more subtile description. At first sight on the 2D map, isolines are almost parallel to the X-axis, suggesting a temperature invariance of R_d. To check this point, Y-error bars have been added to the 0.9 Pa data in Fig. 2. They represent the (Max-Min) variation of the deposition rate with temperature, varying between 250 and 750 °C. At low RF power, there is no dispersion of R_d with varying temperature. When P_{ow} is raised, there is a continuously increasing effect of the substrate temperature, evidenced by a larger error bar. For example, at the highest power, i.e. 450W, a linear decrease of Rd with increasing substrate temperature can be seen (Fig. 3). As the substrate temperature does not affect the ejection rate from the target, it can be stated that an increase of temperature reduces condensation efficiency. The behavior observed shows an increase of the desorption rate from the substrate as the temperature increased. Despite narrower parameter ranges explored, such a weak effect of both pressure and temperature has already been observed [29].

The silicon to carbon (Si/C) ratio was systematically measured by SIMS (Fig. 4). It is the total chemical element content of the films, without considering their chemical bonding environment. Depth pro- files showed no variation of stoichiometry with thickness (see for instance Appendix 2). The maximum error was estimated at 0.0065 on the Si/C ratio from a series of consecutive measurements for each sample (standard deviation). Thus, the error on the Si/C ratio determination was rather low. There was a clear increase of the Si/C ratio with increasing RF power applied to the target. The stoichiometry varied from very slight carbon-rich films at the lowest power (Si/C = 0.968) to silicon-rich films at the highest RF power. The films reached a Si/C = 1.138 at 450 W. These values of the Si/C ratio corresponded to a film composition variation between $Si_{0.49}C_{0.51}$ and $Si_{0.53}C_{0.47}$. A similar trend has already been observed in the literature [30]. Note that the measurements conducted on samples deposited at pressures of 0.1 Pa and 0.5 Pa (not shown here) did not show significant variations of the film stoichiometry at a fixed power, compared to the films

deposited at 0.9 Pa. The same applies for the temperature, which did not show a significant effect. We can thus state that RF power is the main parameter that controls the film stoichiometry. Despite a similar trend has been observed between the deposition rate and Si/C ratio as a function of RF power, R_d is not the parameter that governs the film stoichiometry. Indeed, while for a given RF power, pressure considerably modifies R_d (see Fig. 2), the Si/C ratio is only slightly modified, or even unchanged.

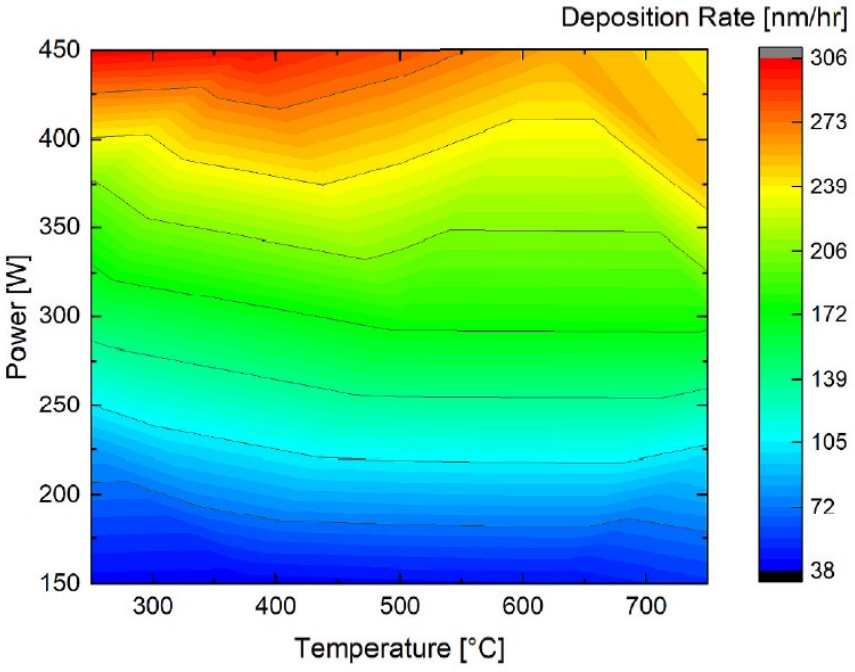

Fig. 1. 2D plot of the deposition rate (R_d) as a function of both temperature (T) and plasma power (P_{ow}). The process pressure is kept at 0.9 Pa.

Moreover, XPS measurements were collected to assess the nature of chemical bonding in the a-SiC films (Fig. 5). The relative contribution of component of the the C–C component to the total C 1s peak ($C–C/C_{tot}$) is plotted as a function of the Si/C ratio determined by SIMS. First, it is worth noting that the data present a strong dispersion. This is the reason why we added a linear fit (regression) and a confidence band, simply as a visual guide to show the trend. This dispersion is the combination of several possible factors. The first one is the reproducibility of the PVD deposition process itself. To assess this effect, a series of 5 similar depositions was performed, with conditions corresponding to the central point of the space parameters; i.e. an RF power of 300 W, a substrate temperature of 500 °C, a pressure of 0.5 Pa and a constant deposition time of 90 min. For this set of experiments, we obtained a deposition rate (R_d) of 303 16 (nm/hr) and a Si/C ratio measured by SIMS of 1.055 ± 0.013; the errors indicated correspond to the standard deviation. The repeatability of the deposition process in terms of R_d and Si/C ratio is thus very good, as shown by the low standard deviation values. The second factor is the accuracy of the XPS quantification, which is usually considered to be in the 10 % range. The third factor could be the amorphous nature of the film:

even with the same flux of atoms impinging the surface (deter- mining both the deposition rate and the Si/C ratio), their chemical structure could vary from one deposition to another. Overall, it appears that the C–C content has a linear dependance with the Si/C ratio. The relative amount of C–C bonds decreases as the Si/C ratio increases. Note that the relative amount of C–Si bonds ($C–Si/C_{tot}$) extracted from the C1s peak, not shown in Fig. 5, increases with an increasing Si/C ratio, as it is the complementary part or the $C–C/C_{tot}$ value, the sum of both being equal to 1. As the stoichiometry progressively shifts towards a Si-rich composition, the probability of producing C–C bonds is lower. In other words, C–C bonds are progressively replaced by C–Si bonds, as seen from the C 1s core level. At Si/C = 1.0, about 24 % of the C 1s peak area is related to C–C bonds, and 76 % to C–Si bonds.

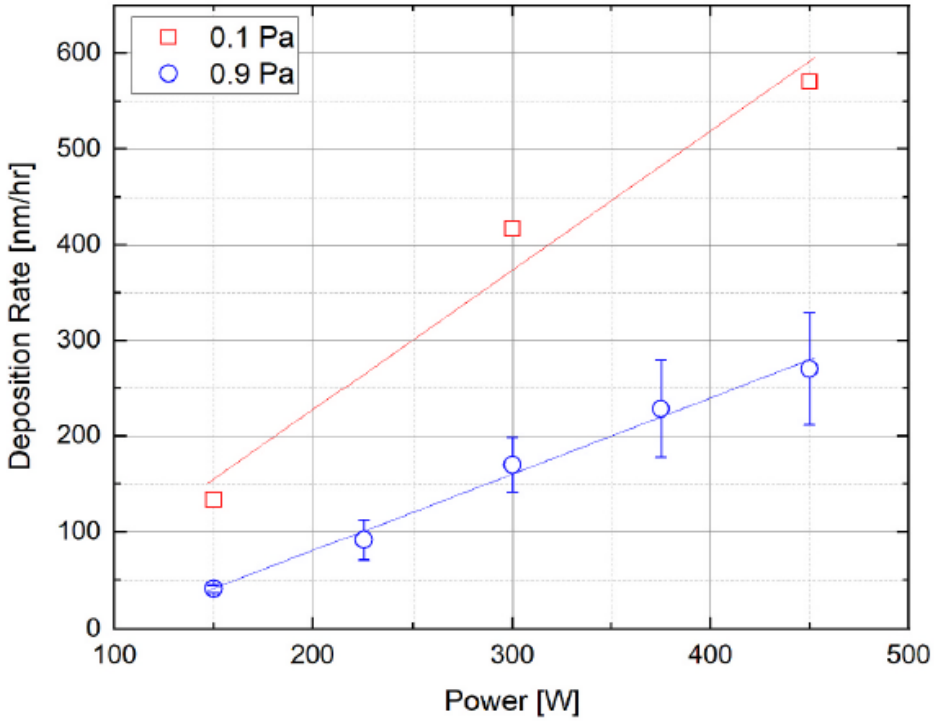

Fig. 2. Deposition rate (R_d) as a function of RF plasma power (P_{ow}) for two different pressures (P_r): 0.1 and 0.9 Pa. The values displayed for each power are average values from a set of experiments. The Y-error bars added to the 0.9 Pa data represent the (Max-Min) variation of the deposition rates with tempera- ture, varying between 250 and 750 °C. Note that these are not the Max and Min values shown in Fig. 3 but the difference, centered on the mean value. Such a specific error bar could thus appear as shifted with respect to the data presented in Fig. 3. The lines are linear regressions of the experimental data.

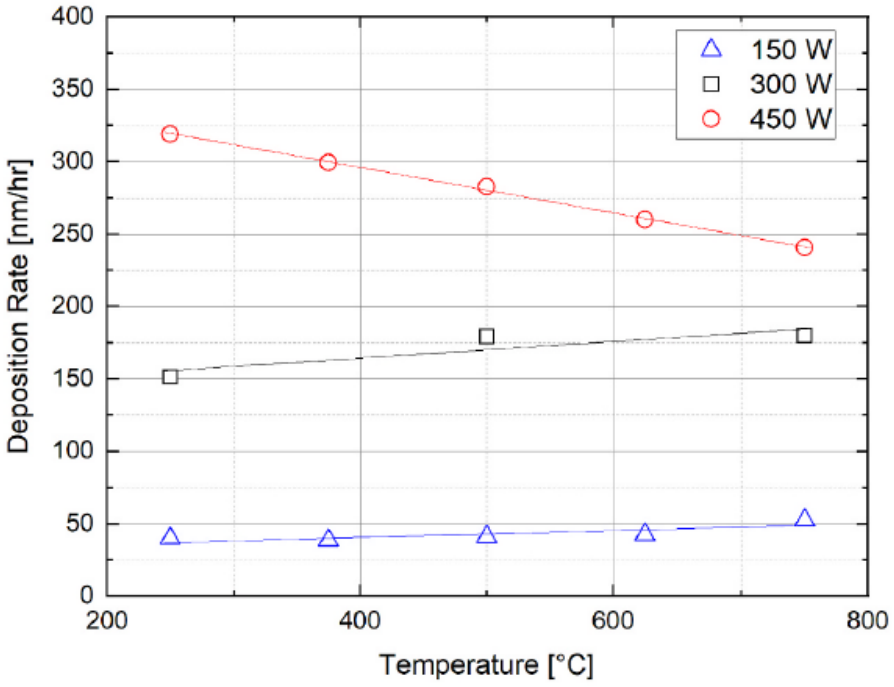

Fig. 3. Deposition rate (R_d) as a function of substrate temperature (T) for three different RF powers (150, 300 and 450W) at a pressure of 0.9 Pa. These data correspond to a part of the different points used to build the "error bar" in Fig. 2.

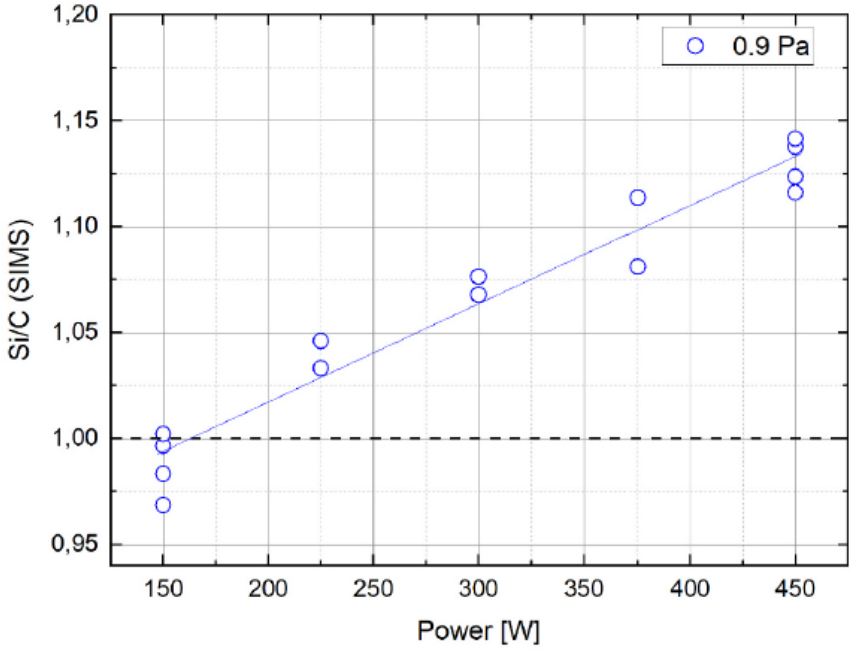

Fig. 4. Stoichiometry of the SiC film (Si/C ratio) measured by SIMS as a function of RF power applied to the target. Only the films deposited at a pressure of 0.9 Pa are represented. The different data shown for a given RF Power correspond to different substrate temperatures. As there was no clear trend on the effect of temperature, we did not differentiate the substrate temperature in this figure.

From a structural standpoint, all the samples did not present any diffraction peak, confirming that the SiC layers grown are amorphous. Fig. 6 presents the X-ray diffraction two dimensional (2D) reciprocal space map of the film deposited at an RF power = 450 W, a pressure of 0.9 Pa and a substrate temperature of 750 °C. Besides the diffraction spots which come from the Si substrate, there is no signature of any other crystalline material. Note that we obtained similar XRD results for all the conditions explored, especially for all the films deposited at 750 °C, the highest temperature accessible with our magnetron sputtering set-up. Fig. 7 shows the Raman spectra of two thin films deposited on sapphire at two different substrate temperatures, 250 °C and 750 °C, all the other parameters being similar. The two samples, deposited at an RF power of 300 W have a very similar Si/C ratio of about 1.072 (averaged value), as measured by SIMS (see Fig. 4). Three obvious broad bands can be observed in the Raman spectra; they can be assigned based on the work of Inoue et al. [31]. At low wave numbers (400-600 cm^{-1}) a weak band associated with Si–Si bonds corresponds to amorphous sili- con. When the deposition temperature increases, this band seems to shift slightly towards higher wave numbers. This had already been seen during a-SiC annealing [32]. The second band which is also very weak, lies between 600 and 1000 cm^{-1}. It is associated with the Si–C bond. Overall, the spectra are dominated by the more intense C–C band in the 1100-1600 cm^{-1} range, which appears as a symmetric single peak, characteristic of amorphous-C. There is no obvious presence of the D (1370 cm^{-1}) and G components (1580 cm^{-1}) whose position, shape and intensity can vary significantly with the structure, the nature of the bonds and the presence of defects in carbon-based materials [33,34]. The band is symmetric and narrow enough to be fitted with only one Gaussian centered around 1450 cm^{-1}. It is thus not possible to apply a similar fitting procedure to that in Ref. [19] and extract information about possible sp^2 and sp^3 carbon content. As mentioned by Baia Neto et al. [32], who observed very similar Raman band for a-SiC:H films, this type of band is attributed to dispersed C–C bonds which do not form graphitic clusters. The presence of this strong C-related Raman band is consistent with the significant concentration of C–C bonds extracted from the XPS C 1s peaks. For the samples shown in Fig. 7, the C–C bond contribution ($C–C/C_{tot}$) measured by XPS is 0.19 and 0.23 for deposition temperature of 250 °C and 750 °C respectively. The area of the C-related Raman bands correlates well with the C–C bond component of the XPS spectra. Unfortunately, a quantitative analysis of the Raman peaks could not be performed at this stage as all the other samples did not have the same thickness.

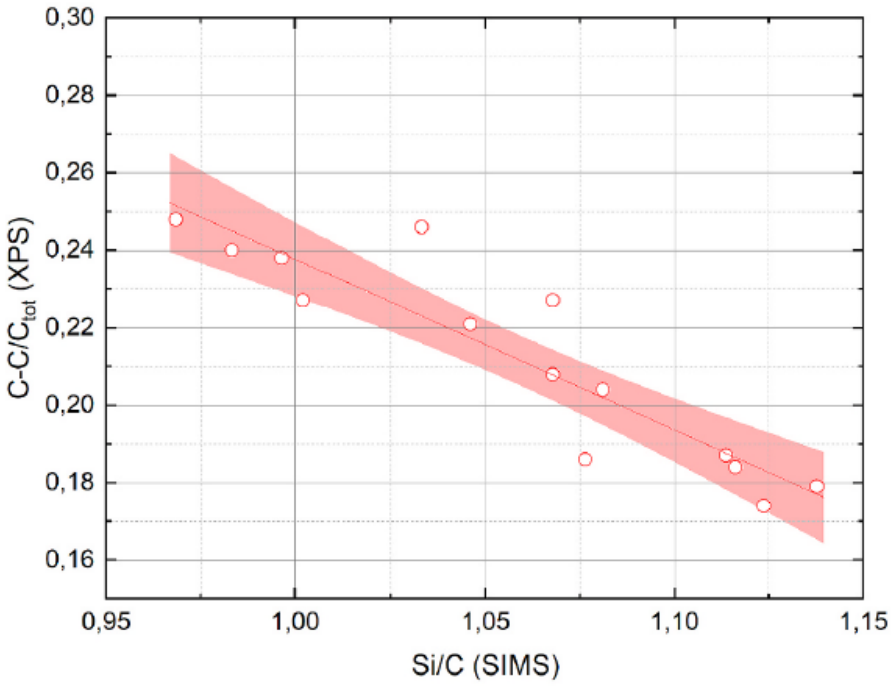

Fig. 5. Chemical analyses of the amorphous SiC films. The X-axis is the Si/C ratio determined by SIMS. It is thus the total Si content to the total C content in the films, whatever the chemical state of their environment. The Y-axis is XPS measurements. The relative concentration of C bound to C (C–C component of the C 1s peak) to the total concentration of C atoms (the whole C 1s peak) is plotted in red.

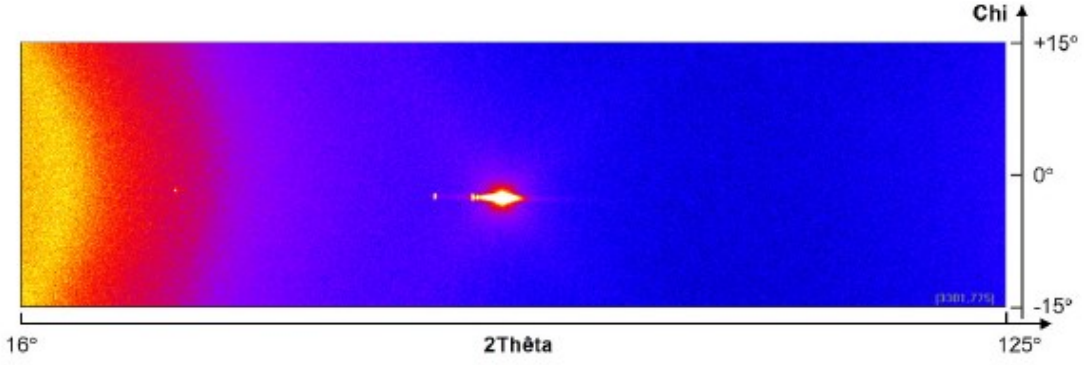

Fig. 6. Typical X-ray 2D reciprocal space map of a 900 nm thick a-SiC film deposited with the following conditions: Pow = 450 W, T = 750 °C, Pr = 0.9 Pa. The diffraction spots correspond to the Si single-crystalline substrate. The corresponding θ-2θ scan is given in Figure A3 in appendix 3.

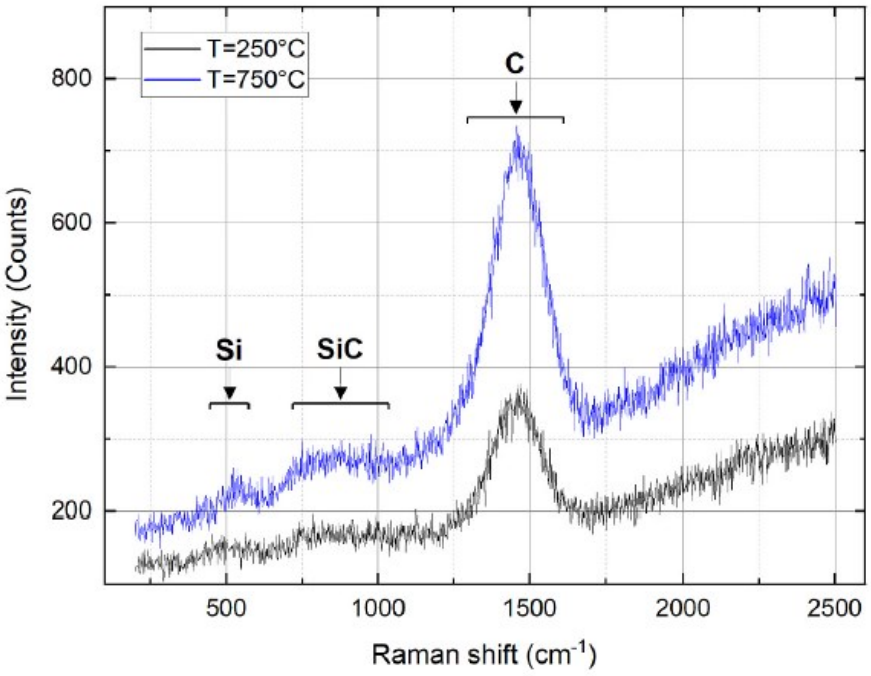

Fig. 7. Raman spectra of two thin films deposited on sapphire, with an RF power of 300 W and a pressure of 0.9 Pa. The films are 250 nm thick, and differ only by the deposition temperatures, which were 250 °C (black spectrum) and 750 °C (blue spectrum). Measurement conditions were similar.

It is worth noting that we observed the same band shape around 1450 cm^{-1} without splitting and without any significant shift whatever the deposition conditions explored. Only the intensity (peak area) varied such as in Fig. 7. This suggests that the concentration of dispersed C–C bonds varies in the films but not the chemical nature or the micro- structure (graphitization, C clustering ….). From that point of view, the behavior of our hydrogen-free a-SiC films considerably differs from the a-SiC:H films deposited by the same method [32,35].

The main optical properties of the a-SiC films have been measured and are gathered in Fig. 8 as a function of the film's Si/C stoichiometry as determined by SIMS. In red (left axis), the refractive index (RI) was measured using spectroscopic ellipsometry. Here, we show only the RI at a wavelength of 1550 nm, as it is the infra-red telecommunication window that motivated this work. In blue (right axis), the optical bandgap (Eg) was extracted from the UV–vis absorption spectra in transmission. The absorbance curves were plotted using the Tauc formalism applied to the indirect bandgap to extract the bandgap value (see Appendix 4). As with Fig. 5, linear trends are observed. A linear fit together with confidence bands have been added to the plots as a visual guide. The refractive index increases from 2.5 to 2.75 when the Si/C ratio changes from 0.96 to 1.14. Conversely, the optical bandgap de- creases from 2.4 to 1.7 eV over the same stoichiometry range. A decrease of optical bandgap with increasing RF power has already been observed [25,36], but not linked to Si/C variations. A similar comment can be done on the refractive index:

its increasing with increasing RF power has already been observed, but not necessarily linked to film composition [25,27].

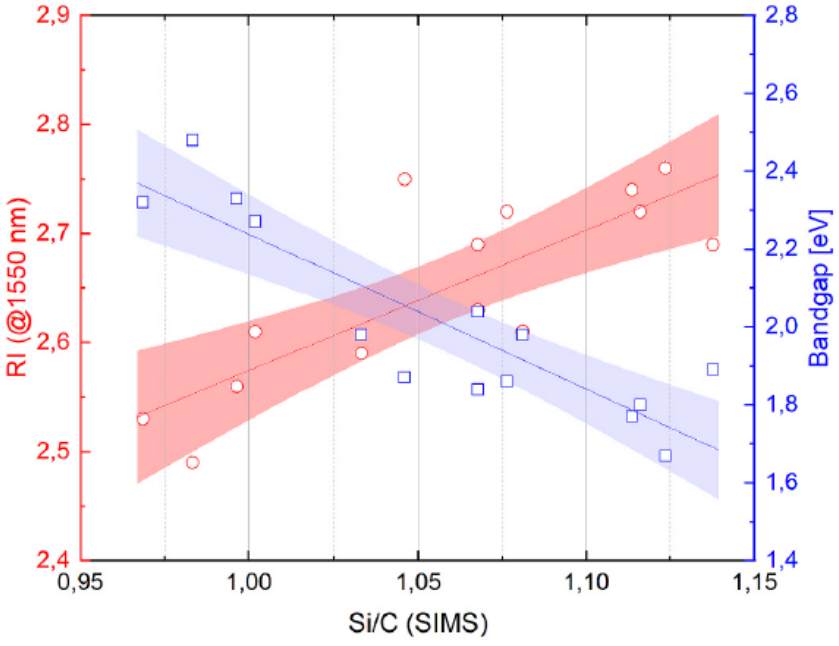

Fig. 8. Refractive index (left axis and red plots) measured by spectroscopic ellipsometry at the wavelength of 1550 nm and bandgap (right axis and blue data), measured in transmission by UV–vis absorption as a function of the film stoichiometry (Si/C ratio measured by SIMS).

We observed the same dispersion in the data as for the C–C con- centration measured by XPS. Here, such dispersion cannot be ascribed to the uncertainty of the measurement tools as both ellipsometry and especially UV–vis spectrometry can provide very accurate values. As already said, the repeatability assessment gave pretty good values with high reproducibility of R_d and film stoichiometry (Si/C ratio measured by SIMS). The dispersion of the values thus occurs in the "chemical structure", i.e. bonding, and the optical properties (RI and Eg) of a-Si_XC_{1-X}. The weak ordering pointed out by Tersoff [16], could give rise to such variability. A combined experimental and theoretical work recently proposed by Favaro et al. [37] also highlighted the strong variability of the optical constants of a-Si_XC_{1-X} films. They suggested that as-deposited thin films are in a non-stabilized state. The authors also demonstrated that a long, low temperature annealing could drastically improve the optical constants.

Cheng et al. suggested the presence of C clusters in RF sputtered amorphous SiC films [19] with a mixture of sp^3 and sp^2 carbon bonding. They also observed a decrease of the Si/C ratio with increasing RF power, with a Si/C ratio very far from stoichiometry (always <0.65), despite the use of a stoichiometric SiC target, which is very different from the literature [14]. In our case, the variability in both the optical constants and the C–C bond content in the a-Si_XC_{1-X} suggests that there are correlated, and that the Si/C ratio does not play the major role, at least for small variations around stoichiometry. For x 0.5 (perfectly stoichiometric

film, as measured by SIMS), Eg is 2.3 eV and the RI (at 1550 nm) is 2.56. The bandgap decreases with decreasing C–C bond content. The single, symmetric and relatively narrow carbon related band in the Raman spectra, without any evidence of band splitting and/or the presence of the usual D and G bands, suggests that our film is highly amorphous, and the presence of graphitic carbon unlikely. This is also supported by the XPS C 1s peak which is also relatively narrow, without any shoulder.

4. Conclusion

Amorphous SiC films were deposited by RF magnetron sputtering using a single source of high-purity polycrystalline SiC. By exploring a three-parameter space (RF power, substrate temperature, pressure), we demonstrated that RF power is the main parameter that, at first order, controls all the deposition process and film properties. By simply adjusting the RF plasma power between 150 and 450 W, it is possible with a Si/C = 1.00 stoichiometric target, to continuously vary the thin film stoichiometry from a C-rich composition ($Si_{0.49}C_{0.51}$) at low power to a Si-rich composition ($Si_{0.53}C_{0.47}$) at high power. This is also associated with a linear variation of the deposition rate (Rd) with the RF plasma power. As all the films are amorphous, it is speculated that the optical properties are closely related to the films' chemical structure, i.e. the nature and concentration of the chemical bonds, and especially to the C–C bond content. By adapting the sputtering conditions, it is therefore possible to very easily tune the refractive index at a wave-length of 1.55 μm in the range 2.50–2.75 and vary the bandgap from 2.5 to 1.7 eV. This will lead to developing an easy method to tune a-Si_XC_{1-X} film using a simple sputtering process for waveguide applications.

Acknowledgements

The authors gratefully acknowledge the support of the European Union's Horizon 2020 FET Open project (SiComb, No. 899679).

Appendix 1

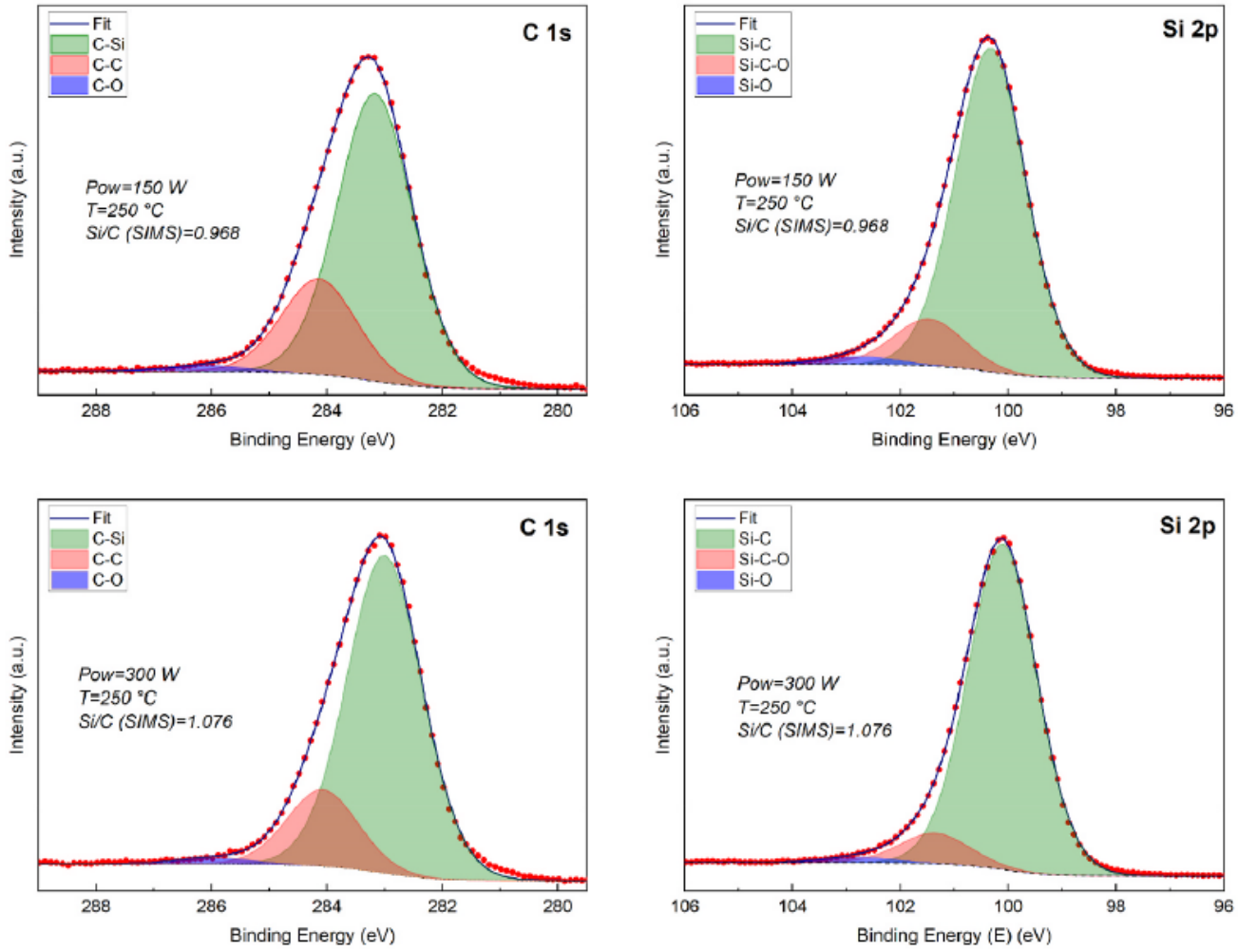

Fig. A.1. Examples of deconvolution of the C1s (left) and Si2p (right) XPS peaks for two different deposition experiments performed at the same substrate tem- perature (250 °C) and pressure (0.9 Pa). The two experiments varied by the RF power applied to the target: 150 W for the first experiment (top) and 300 W for the second (bottom) which produced slightly carbon-rich and slightly silicon-rich films, respectively.

Appendix 2

Figure A.2. a gives an example of a profile resulting from the analysis of a ~275 nm thick SiC layer. The $12C^-$ and $28Si^-$ signal evolutions are plotted as a function of time, from the surface (at time 0 s) up to the interface (at time ~ 1050 s). The Si^-/C^- ratio over the SiC layer can be obtained by dividing the $28Si^-$ signal by the $12C^-$ signal over the sputtering time (see Fig. A2 b). Then, the Si^-/C^- ratio in the stability area located at the center of the plateau is extracted (Si^-/C^- ratio = mean value of the $28Si^-/12C^-$ signal over the stabilized area).

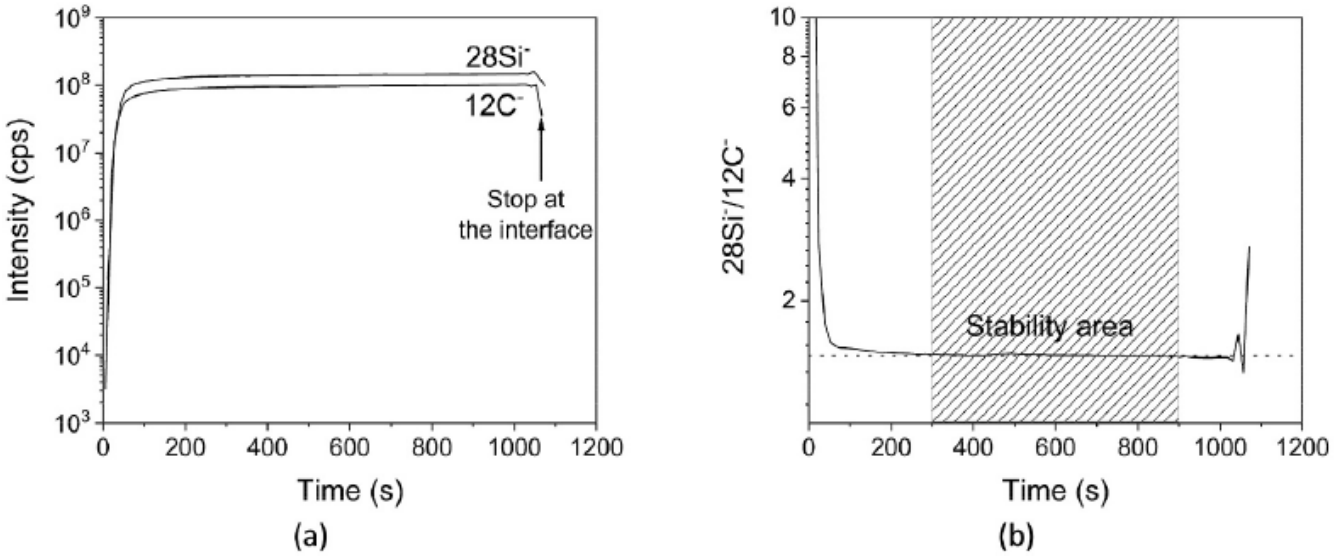

Fig. A.2. (a) SIMS profile (raw data) of a ~275 nm SiC layer with $28Si^-$ and $12C^-$ signals; (b) Profile of the ratio between $28Si^-$ signal and $12C^-$ signal, the dashed rectangle indicates the stability area from which the value of the Si^-/C^- ratio is extracted.

Appendix 3

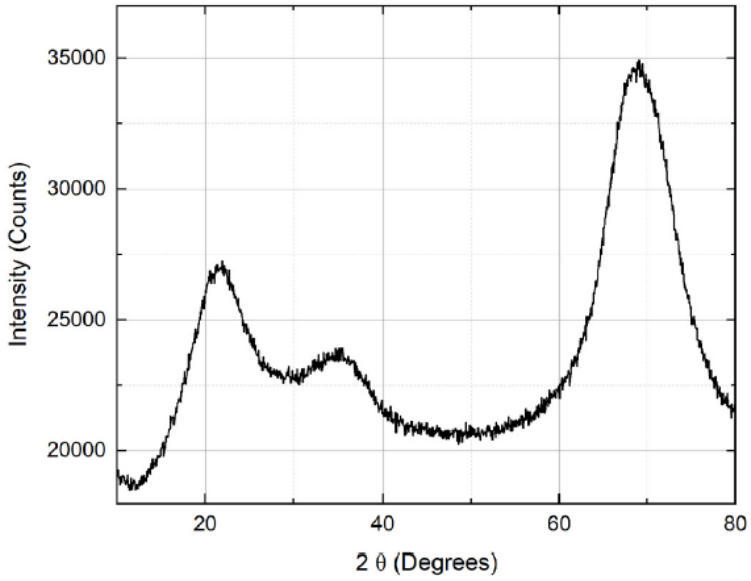

Fig. A.3. Omega-2θ scan of a 900 nm thick a-SiC film deposited with the following conditions: P_{ow} = 450 W, T = 750 °C, P_r = 0.9 Pa. The scan was obtained by a 3° offset along Omega in order to reduce the contribution of the intense peaks related to the Si substrate.

Appendix 4

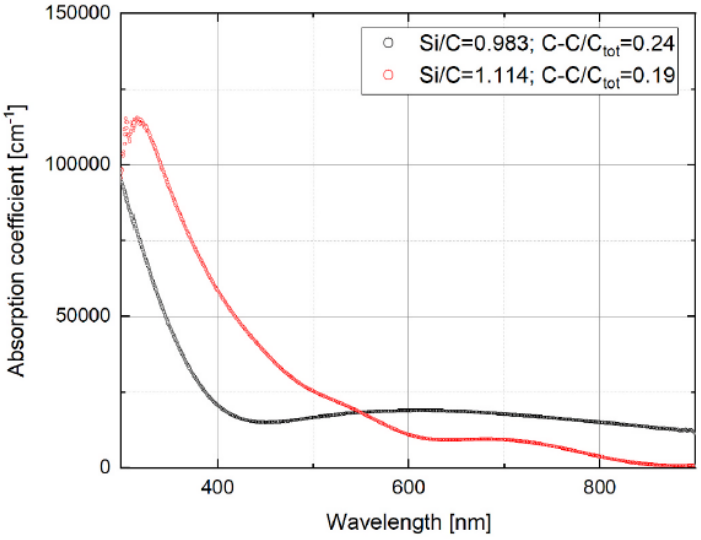

Fig. A.4a. Absorption coefficient as a function of wavelength obtained from UV–vis absorbance spectra, for two different a-SiC films. The two samples selected were deposited using the following conditions: P_r = 0.9 Pa and for red curve: P_{ow} = 375 W and T = 250 °C, for the black curve: P_{ow} = 150 W and T = 625 °C. The corresponding Si/C ratio measured by SIMS and C–C bond content measured by XPS is indicated in the legend.

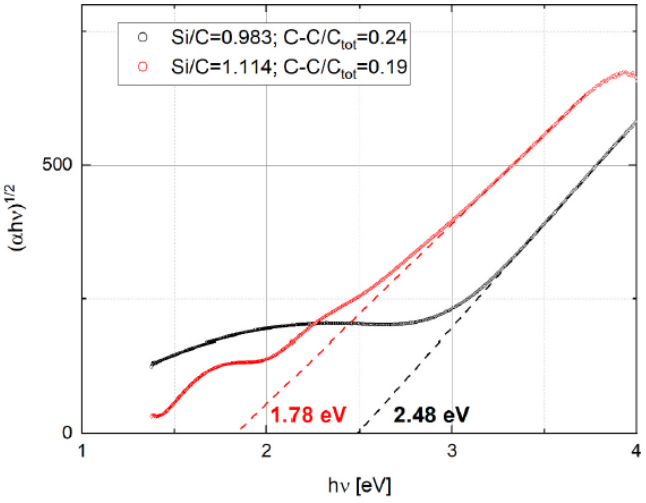

Fig. A.4b. Tauc plots of the two sets of data presented in Figure A4a, considering the bandgap as indirect. The two samples selected were deposited using the following conditions: P_r = 0.9 Pa and for red curve: P_{ow} = 375 W and T = 250 °C, for the black curve: P_{ow} = 150 W and T = 625 °C. The corresponding Si/C ratio measured by SIMS and C–C bond content measured by XPS is indicated in the legend.

References

[1] C.R. Eddy, D.K. Gaskill, Silicon carbide as a platform for power electronics, Science 324 (2009) 1398–1400, https://doi.org/10.1126/science.1168704.

[2] D. Chaussende, N. Ohtani, 5 - silicon carbide, in: R. Fornari (Ed.), Single Cryst. Electron. Mater., Woodhead Publishing, 2019, pp. 129–179.

[3] T. Kimoto, J.A. Cooper, Fundamentals of Silicon Carbide Technology: Growth, Characterization, Devices and Applications, John Wiley & Sons Singapore Pte. Ltd, 2014.

[4] H. Ou, X. Shi, Y. Lu, M. Kollmuss, J. Steiner, V. Tabouret, M. Syväjärvi, P. Wellmann, D. Chaussende, Novel photonic applications of silicon carbide, Materials 16 (2023) 1014, https://doi.org/10.3390/ma16031014.

[5] S. Castelletto, A. Peruzzo, C. Bonato, B.C. Johnson, M. Radulaski, H. Ou, F. Kaiser, J. Wrachtrup, Silicon carbide photonics bridging quantum technology, ACS Photonics 9 (2022) 1434–1457, https://doi.org/10.1021/acsphotonics.1c01775.

[6] Y. Zheng, M. Pu, A. Yi, B. Chang, T. You, K. Huang, A.N. Kamel, M.R. Henriksen, A. A. Jørgensen, X. Ou, H. Ou, High-quality factor, high-confinement microring resonators in 4H-silicon carbide-on-insulator, Opt Express 27 (2019) 13053–13060, https://doi.org/10.1364/OE.27.013053.

[7] X. Shi, Y. Lu, N. Peng, K. Rottwitt, H. Ou, High-performance polarization- Independent beam splitters and MZI in silicon carbide integrated platforms for single-photon manipulation, J. Light. Technol. 40 (2022) 7626–7633.

[8] X. Shi, J. Zhang, W. Fan, Y. Lu, N. Peng, K. Rottwitt, H. Ou, Compact low- birefringence polarization beam splitter using vertical-dual-slot waveguides in silicon carbide integrated platforms, Photon. Res. 10 (2022) A8–A13, https://doi.org/10.1364/PRJ.443543.

[9] X. Shi, W. Fan, A.K. Hansen, M. Chi, A. Yi, X. Ou, K. Rottwitt, H. Ou, Thermal behaviors and optical parametric oscillation in 4H-silicon carbide integrated platforms, Adv. Photon. Res. 2 (2021) 2100068.

[10] M.A. Guidry, K.Y. Yang, D.M. Lukin, A. Markosyan, J. Yang, M.M. Fejer, J. Vučković, Optical parametric oscillation in silicon carbide nanophotonics, Optica 7 (2020) 1139–1142, https://doi.org/10.1364/OPTICA.394138.

[11] K. Powell, L. Li, A. Shams-Ansari, J. Wang, D. Meng, N. Sinclair, J. Deng, M. Lončar, X. Yi, Integrated silicon carbide electro-optic modulator, Nat. Commun. 13 (2022) 1851, https://doi.org/10.1038/s41467-022-29448-5.

[12] Y. Hamakawa, Physics and applications of amorphous silicon carbide, in: M. M. Rahman, C.Y.-W. Yang, G.L. Harris (Eds.), Amorph. Cryst. Silicon Carbide II, Springer, Berlin, Heidelberg, 1989, pp. 164–170, https://doi.org/10.1007/978-3- 642-75048-9_35.

[13] G. Foti, Silicon carbide: from amorphous to crystalline material, Appl. Surf. Sci. 184 (2001) 20–26, https://doi.org/10.1016/s0169-4332(01)00751-6.

[14] J. Bullot, M.P. Schmidt, Physics of amorphous silicon–carbon alloys, Phys. Status Solidi B 143 (1987) 345–418, https://doi.org/10.1002/pssb.2221430202.

[15] S. Greenhorn, E. Bano, V. Stambouli, K. Zekentes, Amorphous SiC thin films deposited by plasma-enhanced chemical vapor deposition for passivation in biomedical devices, Materials 17 (2024) 1135, https://doi.org/10.3390/ ma17051135.

[16] J. Tersoff, Chemical order in amorphous silicon carbide, Phys. Rev. B 49 (1994) 16349–16352, https://doi.org/10.1103/PhysRevB.49.16349.

[17] C.J. Mogab, W.D. Kingery, Preparation and properties of noncrystalline silicon carbide films, J. Appl. Phys. 39 (1968) 3640–3645, https://doi.org/10.1063/ 1.1656832.

[18] Y. He, C. Ye, X. Wang, M. Gao, J. Guo, P. Yang, Structural properties and preparation of Si-rich Si1—xCx thin films by radio-frequency magnetron sputtering,Appl. Surf. Sci. 363 (2016) 477–482, https://doi.org/10.1016/j. apsusc.2015.12.097.

[19] Y. Cheng, X. Huang, Z. Du, J. Xiao, Effect of sputtering power on the structure and optical band gap of SiC thin films, Opt. Mater. 73 (2017) 723–728, https://doi.org/ 10.1016/j.optmat.2017.09.031.

[20] X. Chen, X. Wang, D. Fang, A review on C1s XPS-spectra for some kinds of carbon materials, Fuller. Nanotube, Carbon Nanostruct. 28 (2020) 1048–1058, https:// doi.org/10.1080/1536383X.2020.1794851.

[21] M.A. Pinault-Thaury, F. Jomard, Nitrogen investigation by SIMS in two wide band- gap semiconductors: diamond and silicon carbide, Mater. Sci. Forum 1062 (2022) 376–382, https://doi.org/10.4028/p-684nsi.

[22] H. Tang, S. Tan, Z. Huang, S. Dong, D. Jiang, Surface morphology of β-SIC coatings deposited by RF magnetron sputtering, Surf. Coat. Technol. 197 (2005) 161–167, https://doi.org/10.1016/j.surfcoat.2004.11.036.

[23] A. Sathyamoorthy, W. Weisweiler, Studies of the sputter deposition of carbon, silicon and SiC films, Thin Solid Films 87 (1982) 33–42, https://doi.org/10.1016/ 0040-6090(82)90568-5.

[24] M. Liu, Y. Yang, Q. Mao, Y. Wei, Y. Li, N. Ma, H. Liu, X. Liu, Z. Huang, Influence of radio frequency magnetron sputtering parameters on the structure and performance of SiC films,

Ceram. Int. 47 (2021) 24098–24105, https://doi.org/ 10.1016/j.ceramint.2021.05.120.

[25] J. Keun Seo, K. Ko, W. Seok Choi, M. Park, J. Hwan Lee, J.-S. Yi, The effect of deposition RF power on the SiC passivation layer synthesized by an RF magnetron sputtering method, J. Cryst. Growth 326 (2011) 183–185, https://doi.org/ 10.1016/j.jcrysgro.2011.01.093.

[26] W.K. Choi, F.L. Loo, F.C. Loh, K.L. Tan, Effects of hydrogen and rf power on the structural and electrical properties of rf sputtered hydrogenated amorphous silicon carbide films, J. Appl. Phys. 80 (1996) 1611–1616, https://doi.org/10.1063/ 1.362959.

[27] K.Kh Nussupov, N.B. Beisenkhanov, S. Keiinbay, A.T. Sultanov, Silicon carbide synthesized by RF magnetron sputtering in the composition of a double layer antireflection coating SiC/MgF2, Opt. Mater. 128 (2022) 112370, https://doi.org/ 10.1016/j.optmat.2022.112370.

[28] A.V. Singh, S. Chandra, S. Kumar, G. Bose, Mechanical and structural properties of RF magnetron sputter-deposited silicon carbide films for MEMS applications, J. Micromechanics Microengineering 22 (2012) 025010, https://doi.org/10.1088/ 0960-1317/22/2/025010.

[29] W.K. Choi, F.L. Loo, C.H. Ling, F.C. Loh, K.L. Tan, Structural and electrical studies of radio frequency sputtered hydrogenated amorphous silicon carbide films, J. Appl. Phys. 78 (1995) 7289–7294, https://doi.org/10.1063/1.360377.

[30] S.M. Rajab, I.C. Oliveira, M. Massi, H.S. Maciel, S.G. dos Santos Filho, R. D. Mansano, Effect of the thermal annealing on the electrical and physical properties of SiC thin films produced by RF magnetron sputtering, Thin Solid Films 515 (2006) 170–175, https://doi.org/10.1016/j.tsf.2005.12.052.

[31] Y. Inoue, S. Nakashima, A. Mitsuishi, S. Tabata, S. Tsuboi, Raman spectra of amorphous SiC, Solid State Commun. 48 (1983) 1071–1075, https://doi.org/ 10.1016/0038-1098(83)90834-7.

[32] A.L. Baia Neto, S.S. Camargo, R. Carius, F. Finger, W. Beyer, Annealing effects on near stoichiometric a-SiC:H films, Surf. Coat. Technol. 120–121 (1999) 395–400, https://doi.org/10.1016/S0257-8972(99)00390-4.

[33] A.C. Ferrari, J. Robertson, Interpretation of Raman spectra of disordered and amorphous carbon, Phys. Rev. B 61 (2000) 14095–14107, https://doi.org/10.1103/PhysRevB.61.14095.

[34] S. Reich, C. Thomsen, Raman spectroscopy of graphite, Phil. Trans. Math. Phys. Eng. Sci. 362 (2004) 2271–2288, https://doi.org/10.1098/rsta.2004.1454.

[35] M. Daouahi, N. Rekik, Effect of substrate temperature on (Micro/Nano)Structure of a-SiC:H thin films deposited by radio-frequency magnetron sputtering, J. Phys. Chem. C 116 (2012) 21018–21026, https://doi.org/10.1021/jp3079937.

[36] H. Ferhati, F. Djeffal, A. Bendjerad, L. Foughali, A. Benhaya, A. Saidi, Highly- detective tunable band-selective photodetector based on RF sputtered amorphous SiC thin-film: effect of sputtering power, J. Alloys Compd. 907 (2022) 164464, https://doi.org/10.1016/j.jallcom.2022.164464.

[37] G. Favaro, M. Bazzan, A. Amato, F. Arciprete, E. Cesarini, A.J. Corso, F. De Matteis, T.H. Dao, M. Granata, C. Honrado-Benítez, N. Gutiérrez-Luna, J.I. Larruquert, G. Lorenzin, D. Lumaca, G. Maggioni, M. Magnozzi, M.G. Pelizzo, E. Placidi, P. Prosposito, F. Puosi, Measurement and simulation of mechanical and optical properties of sputtered amorphous SiC coatings, Phys. Rev. Appl. 18 (2022) 044030, https://doi.org/10.1103/PhysRevApplied.18.044030.